J. Fluid Mech. (2007), *vol.* 585, *pp.* 93–115. © 2007 Cambridge University Press
doi:10.1017/S0022112007006568 Printed in the United Kingdom

Wave breaking onset and strength for two-dimensional deep-water wave groups

MICHAEL L. BANNER[1] AND WILLIAM L. PEIRSON[2]

[1]School of Mathematics and Statistics, The University of New South Wales, Sydney 2052, Australia

[2]Water Research Laboratory, School of Civil and Environmental Engineering,
The University of New South Wales, Sydney 2052, Australia

(Received 1 June 2006 and in revised form 8 March 2007)

The numerical study of J. Song & M. L. Banner (*J. Phys. Oceanogr.* vol. 32, 2002, p. 254) proposed a generic threshold parameter for predicting the onset of breaking within two-dimensional groups of deep-water gravity waves. Their parameter provides a non-dimensional measure of the wave energy convergence rate and geometrical steepening at the maximum of an evolving nonlinear wave group. They also suggested that this parameter might control the strength of breaking events. The present paper presents the results of a detailed laboratory observational study aimed at validating their proposals.

For the breaking onset phase of this study, wave potential energy was measured at successive local envelope maxima of nonlinear deep-water wave groups propagating along a laboratory wave tank. These local maxima correspond alternately to wave group geometries with the group maximum occurring at an extreme carrier wave crest elevation, followed by an extreme carrier wave trough depression. As the nonlinearity increases, these crest and trough maxima can have markedly different local energy densities owing to the strong crest–trough asymmetry. The local total energy density was reconstituted from the potential energy measurements, and made dimensionless using the square of the local (carrier wave) wavenumber. A mean non-dimensional growth rate reflecting the rate of focusing of wave energy at the envelope maximum was obtained by smoothing the local fluctuations.

For the cases of idealized nonlinear wave groups investigated, the observations confirmed the evolutionary trends of the modelling results of Song & Banner (2002) with regard to predicting breaking onset. The measurements confirmed the proposed common breaking threshold growth rate of 0.0014 ± 0.0001, as well as the predicted key evolution times: the time taken to reach the energy maximum for recurrence cases; and the time to reach the breaking threshold and then breaking onset, for breaking cases.

After the initiation and subsequent cessation of breaking, the measured wave packet mean energy losses and loss rates associated with breaking produced an unexpected finding: the post-breaking mean wave energy did not decrease to the mean energy level corresponding to maximum recurrence, but remained significantly higher. Therefore, pre-breaking absolute wave energy or mean steepness do not appear to be the most fundamental determinants of post-breaking wave packet energy density.

However, the dependence of the fractional breaking energy loss of wave packets on the parametric growth rate just before breaking onset proposed by Song & Banner (2002) was found to provide a plausible collapse to our laboratory data sets, within the experimental uncertainties. Further, when the results for the energy loss rate per unit width of breaking front were expressed in terms of a breaker strength parameter b multiplying the fifth power of the wave speed, it is found that b was also strongly correlated with the parametric growth rate just before breaking. Measured values of b obtained in this investigation ranged systematically from 8×10^{-5} to 1.2×10^{-3}. These are comparable with open ocean estimates reported in recent field studies.

1. Introduction

Breaking of dominant ocean wind waves in the form of large whitecaps is a familiar occurrence associated with strong wind forcing conditions at sea. Through their overturning of the air–sea interface, such breaking events (as well as those of shorter breaking waves) profoundly influence the dynamics and thermodynamics of the upper ocean and marine atmospheric boundary layer, while their impact forcing provides the greatest safety challenge to offshore shipping and coastal structures. Consequences of breaking in the upper ocean surface layer include greatly enhanced turbulence dissipation rates in the near-surface region (e.g. Terray *et al.* 1996; Gemmrich & Farmer 2004). In the atmospheric marine boundary layer, increased waveform drag can result from the separated air flow over breaking waves, together with augmented sea spray, bubbles and acoustic underwater noise, as well as enhanced microwave backscatter and emissivity. These numerous and diverse aspects of wave breaking are described in greater detail in, for example, Banner & Peregrine (1993); Thorpe (1993) and Melville (1996).

Despite the widespread occurrence of breaking waves at sea, an understanding of the mechanisms that determine the onset and strength of breaking events has been elusive ever since water waves have been studied scientifically. Identifying a robust threshold variable that determines the onset of breaking for deep-water waves has remained a problem for many decades. Various breaking threshold criteria have been proposed based on local wave geometrical or kinematical properties such as wave steepness, crest fluid velocities and acceleration, and Stansell & MacFarlane (2002) provides a critical appraisal of this kinematic approach. However, breaking criteria based on such local properties do not appear to be universally applicable, as evidenced in a number of laboratory and field observations. For example, the comprehensive field study of Holthuijsen & Herbers (1986) highlights the inability to distinguish breaking events on the basis of local wave steepness. In any event, it may be argued that such breaking criteria do not provide much insight into the underlying dynamics that determines the onset and strength of wave breaking, a shortcoming shared by statistically based, broader spectral variants of these criteria (e.g. Papadimitrakis *et al.* 1988).

Of potential significance to the dynamics underlying wave breaking have been field observations associating wave breaking with wave group structure, particularly those of Donelan, Longuet-Higgins & Turner (1972) and subsequently Holthuijsen & Herbers (1986). Furthermore, wave group structure is a conspicuous feature of ocean wave height records and a significant amount of literature exists on this topic. In the present context, the statistics of wave groups (e.g. Longuet-Higgins 1984) and the occurrence of extreme waves in wave groups (e.g. Phillips, Gu & Donelan 1993; Osborne, Onorato & Serio 2000) are of particular relevance. Complementary laboratory observational studies have investigated the unforced (zero wind) evolution of two-dimensional nonlinear wave groups (e.g. Melville 1982, 1983; Rapp & Melville 1990; Kway, Loh & Chan 1998; Tulin & Waseda 1999). These papers, however, do not address the underlying dynamical underpinnings of wave breaking onset. There has also been strong interest in studying nonlinear modulational processes through model equations, such as the nonlinear Schrödinger equation and its higher-order variants (e.g. Dysthe 1979; Dias & Kharif 1999). While well-suited to examining many aspects of wave group behaviour, such model equations cannot describe the onset of wave breaking, which requires the exact (Euler) equation formulation with fully nonlinear free-surface boundary conditions.

Complementary to these theoretical developments, recent numerical studies have been made of the evolution of unforced two-dimensional nonlinear wavetrains beyond the linear perturbation instability stage. These calculations reveal a complex evolution to recurrence or breaking that highlights the fundamental role played by nonlinear intra-wave group dynamics (e.g. Dold & Peregrine 1986; Tulin & Li 1992; Banner & Tian 1998).

The present laboratory investigation seeks to advance present understanding of two fundamental aspects of group-related deep-water wave breaking behaviour: breaking initiation, and subsequent loss of energy from the wave field.

1.1. *Onset of wave breaking*

Song & Banner (2002 hereinafter referred to as SB) used a wave-group-following (WGF) approach to investigate numerically the evolution of unforced two-dimensional nonlinear wave groups with different initial wave group structure. SB sought to identify the difference between evolution to recurrence and to breaking onset, in terms of the rate of mean wave energy convergence and geometrical steepening at the maximum of wave groups, when travelling with these wave group maxima. After calculating the long-term evolution of the maximum of the local energy density of wave groups, with suitable post-processing they tracked the envelope maximum of the wave group energy and calculated an associated non-dimensional parametric mean growth rate δ, defined by

$$\delta(t)=\frac{1}{\omega_c}\frac{\mathrm{D}\langle\mu\rangle}{\mathrm{D}t}, \tag{1}$$

where $\mathrm{D}/\mathrm{D}t$ is the rate of change following the wave group whose initial mean carrier wave frequency is ω_c, $\mu=Ek^2$ is a non-dimensional variable reflecting the local wave energy and wavenumber behaviour. Here, E is the depth-integrated local total energy density (after division by $\rho_w g$) and k is the local wavenumber. The local mean value of μ averaged over several carrier wave periods is denoted by $\langle\mu(t)\rangle$. Following SB, ω_c was taken as the mean frequency of the two spectral modes in case II wave groups and as the mean paddle frequency (ω_p) for the case III wave groups. Definitions of these wave group geometries are given in § 2.2. The mean carrier wave period $T=2\pi/\omega_c$.

The growth rate δ reflects a mean energy convergence rate towards, or away from, the wave group energy maximum, associated with nonlinear interactions of wave energy from other parts of the wave group, as measured by an observer travelling with the wave group. It also reflects the steepening of the maximal carrier waveform associated with the increased local carrier wavenumber. However, as discussed in detail in § 4b of SB, the energy maximum of a wave group oscillates as it grows during the evolution, owing to the crest–trough asymmetry associated with Stokes waves, and these fast oscillations must be filtered out to obtain the associated mean parametric growth rate δ. For the ensemble of different structures and sizes of wave groups they investigated, SB found that this dynamically based mean growth rate had a common threshold of $[1.4\pm0.1]\times10^{-3}$ that distinguished evolution of the group to recurrence without breaking, from evolution in which initiation of breaking occurs. In a companion paper, Banner & Song (2002) extended that unforced study to strongly wind-driven cases, reporting that the hydrodynamics of nonlinear wave groups continued to dominate the breaking onset process even for relatively strong wind forcing. Compared to previously proposed breaking thresholds, this dynamically based approach contributes a more complete physical perspective, both long-term and short-term, of the evolution to breaking and provides an earlier and more decisive indicator for the onset of breaking.

The present paper describes the results of our detailed laboratory study to validate the proposed SB breaking threshold growth rate and their suggested dependence of breaking energy loss on this growth rate just before breaking onset. To this end, detailed measurements were made of the evolution of the wave potential energy density and relevant carrier wave properties in a laboratory wave flume for two representative paddle-generated initial wave group geometries. The experiments were designed to reproduce conditions representing a subset of those in the calculations of SB. From this data, the behaviour of the SB parametric growth rate parameter δ was calculated using exactly the same methodology as in SB for direct comparison with their model results for breaking onset.

1.2. *Strength of wave breaking*

SB also proposed that the growth rate δ_{br} just prior to breaking onset might provide a dynamically based measure of the strength of breaking events, but the latter was not available from their computations, which terminated just after the actual onset of breaking. The consequences of wave breaking remain major challenges in air–sea interaction modelling. We sought to extend present knowledge of breaking energy losses and loss rates beyond their dependence on the initial mean wave packet steepness, as explored by, for example, Dold & Peregrine (1986), Thorpe (1993) and Melville (1994). To this end, we undertook a systematic study of how the post-breaking mean wave packet energy was correlated with the pre-breaking growth rate δ_{br} explored by SB.

For the post-breaking phase, we also examined the breaking energy loss rate relationship proposed by Duncan (1981, 1983). Based on dimensional considerations, Duncan proposed that the energy loss rate per unit width of breaking front ε_L could be expressed in terms of a breaker strength coefficient b multiplying the fifth power of the breaking wave speed c_{br}:

$$\varepsilon_L = b_{br}\rho_w c_{br}^5/g, \tag{2}$$

where ρ_w is the water density. In (2), the unknown non-dimensional coefficient b_{br} reflects the breaking ‘strength’ or ‘intensity’. Subsequent investigations have sought to quantify b_{br} and its parametric dependence (e.g. Phillips 1985; Melville 1994; Peirson & Banner 2000; Phillips, Pasner & Hansen 2001; Melville & Matusov 2002; Gemmrich 2005). Present estimates for the breaking strength coefficient b_{br} from laboratory and field measurements range over two orders of magnitude. From measurements of energy dissipated and breaker durations in the laboratory study of Loewen & Melville (1991), Melville (1994) reported a parametric dependence for b_{br} on the maximum packet wave slope parameter S, where $S=(\Sigma a_n)k_c$ is the maximal steepness of the discrete Fourier wave amplitudes a_n in the wave packet, and k_c is the mean packet wavenumber.

In the present study, we sought to refine the quantification of the breaking strength coefficient b_{br}, particularly its correlation with S and with the more intrinsic breaking parameter δ_{br}. In the following sections, we describe the experimental facilities and

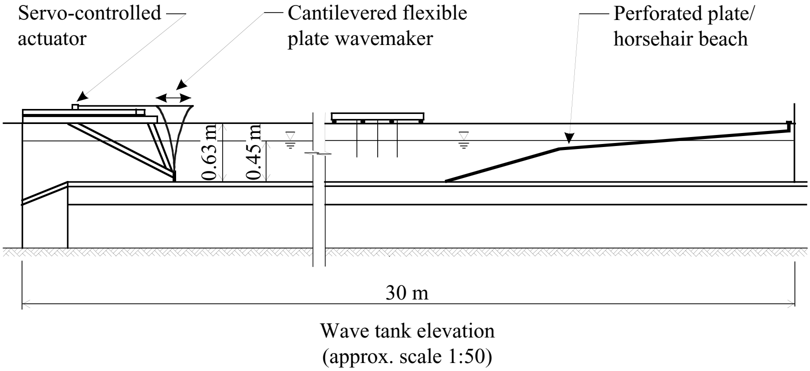

FIGURE 1. Geometrical details of the 30 m wave flume used in the present study. The width of the tank was 0.6 m. The traversing wave probe assembly showing the relative probe positions is shown schematically, with further details given in the text.

techniques used during this investigation, discuss the results obtained, summarize our conclusions and recommendations for future work.

2. Measurement details

As highlighted above, SB used a wave-group-following approach to investigate numerically the evolution of unforced two-dimensional nonlinear wave groups with different initial wave group structure, and the same approach was implemented in the present measurements. This study sought to reproduce conditions typical of those in SB and then determine the location of successive crest and trough wave group maxima as the wave groups evolved along the tank. This was a laborious task, as it had to be done for each of the initial carrier wave steepness cases investigated. Once these maxima were located and the relevant wave measurements recorded, data analysis was undertaken to validate experimentally: (i) the generic breaking threshold behaviour determined by SB; (ii) whether the growth rate δ_{br} just prior to breaking onset correlated with observed energy losses and/or loss rates associated with breaking.

2.1. *Wave tank*

The experiments were carried out in a wave flume (30 m long, 0.6 m wide and 0.6 m high) with glass sidewalls, located at the University of New South Wales Water Research Laboratory, Manly Vale. A programmable servo-controlled actuator drove a flexible plate wave paddle cantilevered from near the tank floor, generating the desired initial wave group structures with excellent repeatability and long-term stability (figure 1). We checked carefully that the wave packets generated were closely two-dimensional and that there were minimal reflections from the downstream absorbing beach. This involved ensuring that the choice of primary carrier wave frequency did not lead to the generation of cross-tank waves at the paddle, and also fine-tuning the beach geometry to minimize spurious reflections. We believe that the observed low background level of low-frequency wave energy that could not be entirely suppressed was due to the bound long waves associated with wave groups. This residual amounted to a background amplitude oscillation of O(1–2 mm) and was regarded as acceptable in relation to the typical carrier wave amplitudes of 20–50 mm used in this study.

There was an associated residual lateral sloshing inhomogeneity of the same order, with $O(1\text{–}2\,\mathrm{mm})$ amplitude.

2.2. *Cases of initial wave groups investigated*

We investigated cases based on two of the generic wave group structures reported by SB. Because of finite tank length considerations, we chose the bimodal initial spectrum (case II) and the chirped wave packet (case III), and initially investigated cases comprising five carrier waves in the initial spatial wave group. The case II wave groups generated had an initial spectrum of the form

$$\eta = a_0 \cos(k_0 x) + \varepsilon a_0 \cos\left(\frac{N+1}{N} k_0 x - \frac{\pi}{18}\right) \quad \text{with } \varepsilon = 1, \tag{3}$$

where a_0 is the amplitude and $N=5$ is the number of waves in the group. The small phase shift, retained from Banner & Tian (1998), is inconsequential. Because of the well-known dispersive properties of deep-water gravity waves, the temporal signal has 10 waves/group to generate this five-wave spatial group structure. With an appropriate mean carrier wave frequency of 1.7 Hz, we were able to match closely the computed wave group evolution within the constraints of our wave tank. We subsequently carried out measurements using a bimodal spectrum with $N=3$ in order to extend our measurement parameter space.

The case III wave groups had a more rapidly deforming geometry characteristic of chirped wave packets where the carrier waves in the packet coalesce rapidly owing to their different phase velocities. These wave packets were produced here, as with the chirped packets in SB, by driving the wavemaker with the motion

$$x_p = -0.25 A_p \left(\tanh \frac{4\omega_p t}{N\pi} + 1\right)\left(1 - \tanh \frac{4(\omega_p t - 2N\pi)}{N\pi}\right) \sin[\omega_p (t - 0.018 t^2/2)], \tag{4}$$

where t is time and N sets the number of carrier waves in the packet, A_p is proportional to the piston amplitude, $\omega_p = (g/(2\pi/\lambda)\tanh((2\pi/\lambda)h))^{1/2}$ is its angular frequency, λ is the wavelength and h is the still-water depth. To simulate deep water, SB took the still-water depth near the wave paddle as $h=4\,\mathrm{m}$, with $\lambda = 2\,\mathrm{m}$. For the case III measurements, we chose a paddle frequency ω_p comparable with the case II waves and used this in (3), as our tank was too short to accommodate the anticipated evolution of a wavelength of $\lambda = 2\,\mathrm{m}$.

We note that the wave paddle mechanism installed in our facility was a bottom-cantilevered flexible plate with tapered stiffness, designed to be optimal for producing deep-water waves with minimal settling distance. This was ideal for simulating the conditions of the case II (periodic domain) wave group evolution. However, it appears to have created a mismatch for the case III wave groups, for which the SB model used a horizontal piston flat-plate paddle motion. We believe that this did not allow us to reproduce optimally the observational conditions for the case III wave groups with the initial conditions of the SB model. The cantilevered flexible-plate generator provides water particle orbital motions far closer to the exponentially decreasing with depth distribution of deep-water waves than horizontal displacement flat-plate generators, which are much better matched to the depth-independent horizontal motion of shallow-water waves. This latter paddle type would therefore be expected to have a longer relaxation distance for the waves to adjust to the deep-water conditions in our tank. As it was not logistically feasible to change the paddle during our experimental programme, we decided to use this case primarily to verify the breaking onset and strength hypotheses of SB, and not for validating evolution details of the modelled case III wave packets. In our experiments, we used (4) with a shorter wavelength of 0.92 m as input for the case III wave groups, which corresponds to a paddle frequency $\omega_p = 8.18\,\mathrm{rad\,s^{-1}}$. Under the circumstances, we felt that this was an appropriate strategy as we were interested primarily in whether a typical evolving chirped wave packet would conform to the generic breaking onset threshold growth rate and energy loss criteria proposed by SB.

2.3. *Wave probes*

After an extensive effort to optimize the two-dimensionality and residual background disturbances from reflections, we settled on an array of six capacitance wave wire gauges with 200 mm elements, configured as two in-line sets of three probes with an inter-probe streamwise spacing of 80–90 mm. This was the minimum separation achievable with the probe electronics casings and represents about 0.1 of the carrier wavelength. The two sets of three probes had a lateral spacing between them of 120 mm. They were mounted on a sliding trolley symmetrically about its centreline, with a 240 mm distance to either tank sidewall. This traversing arrangement allowed the probes to be positioned repeatably to within 5 mm at any location along the tank. The probe resolution was better than 0.1 mm and their linearity was better than ± 1 % of their 200 mm range. They had excellent long-term stability, as demonstrated by approximately monthly static calibrations. This wave probe arrangement allowed the efficient gathering of data for locating the fetches of the local crest and trough maxima of the evolving wave group, and the local surface elevation at these maxima. From this data, the local depth integrated potential energy and the corresponding local wavenumber could be calculated as explained in § 2.5.

2.4. *Frictional losses*

As observed in Rapp & Melville (1990), frictional losses are likely to be significant in this study owing to the tank sidewall separation of 0.6 m. This aspect is discussed in § 4.2 for breaking initiation, and in § 4.3 in connection with breaking losses and loss rates.

We note that well after the conclusion of the main experiments, we were able to repeat one of the runs (case II, $N = 3$) in a 20 m wide wave basin, equipped with a programmable piston paddle. In this wide basin, the viscous losses associated with the tank boundaries were negligible. This provided a valuable opportunity to examine the impact of viscosity on the modulational evolution to breaking initiation, and on the breaking loss and loss rates.

2.5. *Methodology*

We had intended to make particle image velocimetry (PIV) measurements of the subsurface velocity field in order to obtain the depth-integrated kinetic energy density. However, this did not prove to be a feasible option in our wave tank owing to the residual cross-tank variability and difficulty in accurately extracting the dominant wave velocity components very close to the instantaneous free surface. Instead, following Rapp & Melville (1990), we limited our wave energy measurements to the potential energy density, and inferred the kinetic energy densities from the observed potential energy densities based on their relative magnitudes as determined in SB. Therefore, the primary measurements required for the breaking onset phase of this study were the set of wave elevations z_{max} and corresponding wavenumber k_{max} determined at the local successive crest and trough maxima of the wave groups as they evolved with distance from the wave paddle. The potential energy density at these envelope maxima was $gz_{max}^2/2$.

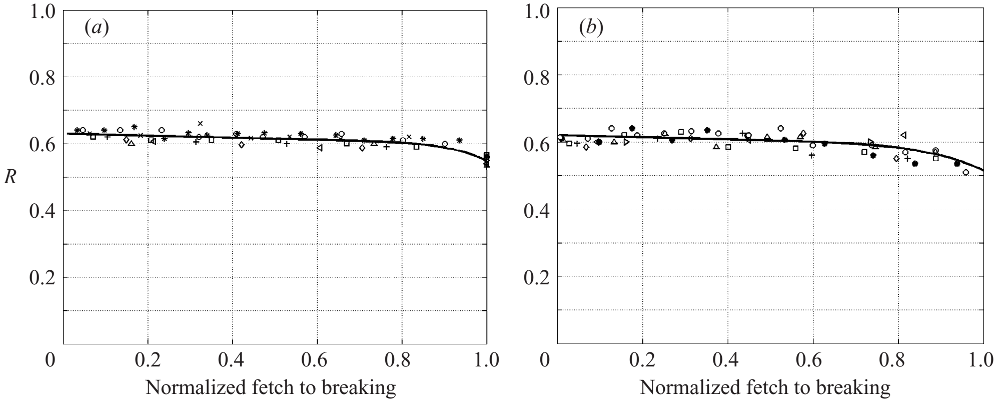

FIGURE 2. Ratio of potential to total energy at local energy maxima during the evolution. (*a*) crest maxima, (*b*) trough maxima. The results shown are for the ensemble of case II, $N = 5$ and case III, $N = 5$ results given in table 1 in SB, where the various symbols represent each of the different initial steepness values. The abscissa is the normalized fetch (or equivalent time) from the paddle to the location of breaking initiation.

The justification for this approach is based on the results of Skyner (1996), who concluded that the internal velocities in similar plunging breakers determined from the Dold–Peregrine code and measured by PIV in a laboratory wave tank agreed within 2 %, even in the overturning spout. The same code was used to generate the data in figure 2 for the ratio of potential to total energy beneath the envelope maximum. Hence, we believe that the model calculations we used to recover the kinetic energy contribution are likely to approximate within a few per cent, results based on measured subsurface velocities. The 'scatter' in the computation for the different cases investigated is seen in figure 2 to be relatively small, and the overall effect on the ratio develops only a relatively modest perturbation as breaking onset approaches and the kinetic energy growth outpaces the potential energy growth. However, from the numerical results, this aspect of the breaking process underpins the common breaking threshold for the range of cases investigated by SB. The other motivation for including the kinetic energy is the complementary goal of parameterizing the breaking strength in terms of the growth rate δ_{br} just prior to breaking initiation.

3. Data acquisition and processing

3.1. *Breaking onset*

As discussed in § 1.1, the goal was to measure the non-dimensional mean growth rate δ, defined by (1). As stated above, the total wave energy density was inferred carefully from the measured potential energy density, based on rescaling it according to the ratio calculated in the SB experiments. These details were kindly provided by J. Song (personal communication). Figure 2 shows the results for the ratio of potential energy density to total energy density from these computations, including the curves representing the conversion formula for crest and trough maxima. For further details on the crest and trough maxima, see the discussion in § 4 of SB.

The determination of the local wavenumber k was made by pairwise Hilbert transform analysis of the signals from the left-hand side set of three wave probes, and similarly from the right-hand side set of probes. The phase function φ for each

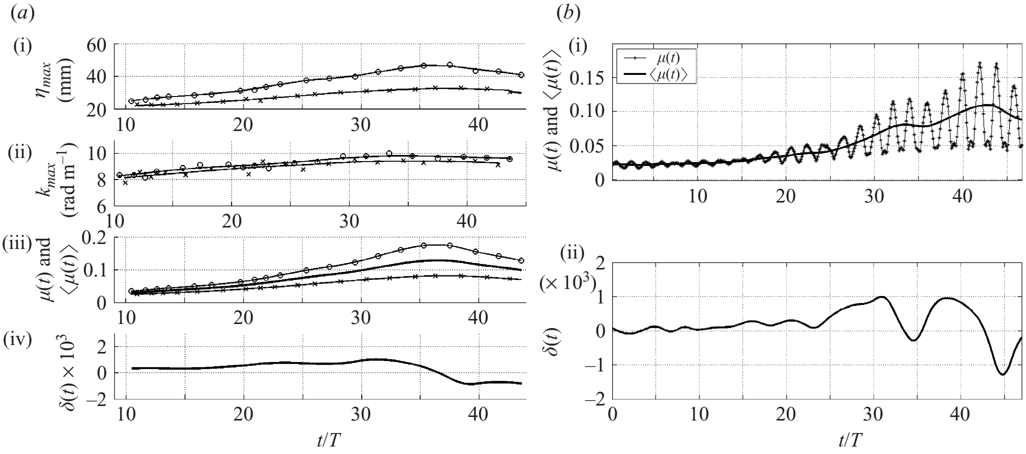

FIGURE 3. (a) Measured evolution properties with fetch, transformed to t/T, for the maximum recurrence case II, $N = 5$ wave groups. (i) Carrier wave height at crest maxima (upper curve) and trough maxima (lower curve). (ii) Corresponding local wavenumber, smoothed as described in the text. (iii) Corresponding evolution of $\mu(t) = Ek^2$ using the group velocity, with crest maxima (upper curve) and trough maxima (lower curve). The central curve is the mean $\langle\mu(t)\rangle$ of the upper and lower curves. (iv) Non-dimensional mean growth rate $\delta(t)$, the normalized derivative of $\mu(t)$, representing the convergence rate of wave energy to the envelope maximum. (b) the corresponding case computed in SB. (i) $\mu(t)$ and $\langle\mu(t)\rangle$, (ii) The corresponding $\delta(t)$.

probe was computed and k determined from any pair of streamwise probes from the relationship $k = \partial\varphi/\partial x$, using the measured phase difference and separation between the two probes. With the ‘satellite’ probes located approximately 80 mm upstream and downstream of the central probes, reliable estimates of the local wavenumber and the local variability could be obtained. The local wavenumber estimated in SB involved low-pass filtering the k distribution along the wave group, with the goal of matching the filtered k-value with the local zero-crossing analysis wavenumber. SB discusses this briefly, but Banner & Tian (1998, § 2.3.4), describes this in greater detail. In the present observational study, we followed the same approach, except that the low-pass filtering was done in the time domain. The-low pass cutoff was set to provide k_{max} values in the range $1 < k_{max}/k_{lin} < 1.3$, as determined in Banner & Tian (1998) and SB. Here, k_{lin} is the nominal mean wavenumber determined from ω_c using the linear deep-water gravity wave dispersion relation. Results for the variation of the local wavenumber following the envelope maximum are shown for the case II, $N = 5$ maximum recurrence wave group case in figure 3, and for the marginal breaking case in figure 4. These figures also allow a detailed comparison to be made of the resulting total wave energy density with the SB computational results.

These figures confirm that our observational procedure was robust. The detailed results are discussed in § 4, which also presents and discusses the full set of results for the various initial wave steepness cases investigated.

3.2. *Post-breaking energy losses and loss rates*

The mean total wave energy $\langle E\rangle$ averaged over a wave group has been chosen as the basis for quantifying the mean breaking energy loss and associated loss rate. To construct the mean total energy from the mean potential energy measured in this study, we again drew on the results of numerical computations in SB. From those

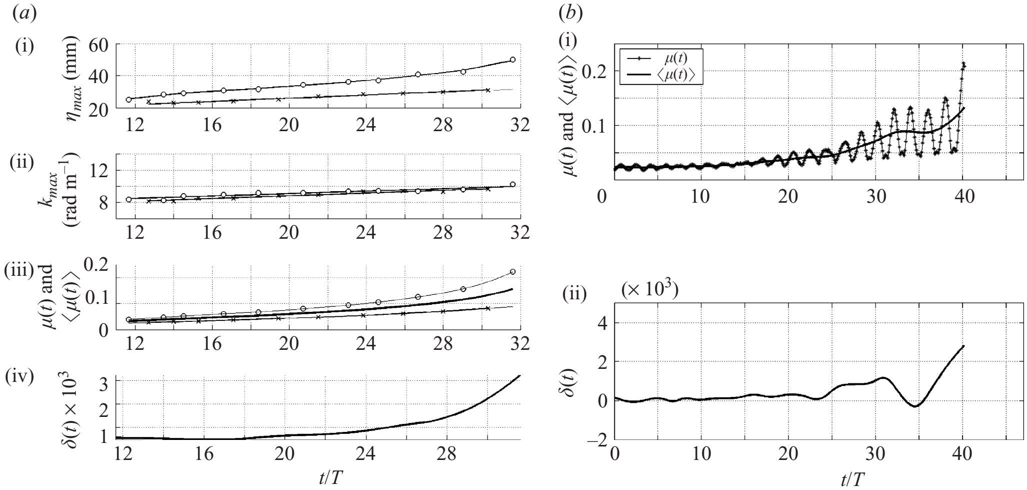

FIGURE 4. As in figure 3, but for case II, $N = 5$ marginal breaking wave groups. (*a*) The observations in this study; (*b*) the corresponding case computed and presented in SB.

calculations, the ratio of mean kinetic energy to mean total energy was found to be 0.505 ± 0.005, i.e. very close to equi-partitioning (J. Song, personal communication).

Measurement of mean potential energy loss rates in this study had to take into account the routine occurrence of successive (multiple) breaking events along the fetch, rather than a single break. This phenomenon has been reported previously both in the field (e.g. Donelan *et al.* 1973) and in the laboratory (e.g. Melville 1996). What determines its occurrence is not yet resolved, but may be associated with the chirp bandwidth, which controls the coalescence rate of the different modes in the nonlinear wave packet (e.g. see Rapp & Melville 1990). Casual observation at sea suggests that even under moderate wind forcing, successive breaking events associated with an identifiable wave packet occur routinely, with single breaking events occurring much less frequently.

In any event, we measured the change of mean potential energy density of the wave packets with distance from the paddle, and extrapolated to obtain the mean total energy density as described above. This provided estimates of the total mean wave energy decay rate associated with the breaking events, together with that due to viscous action within the surface and sidewall boundary-layers. We also routinely measured the location of the start and finish of each of the successive breaking events. We then subtracted the background decay rate due to viscous boundary-layer damping (sidewalls, surface layer and bottom), determined from the data prior to breaking onset, and determined the overall energy loss systematically as a function of δ_{br} and also of the initial maximum steepness S of the wave groups. For S, we followed the definition proposed by Melville (1994), which is based on the product of the mean wavenumber of the group and the sum of the specified Fourier amplitudes of the water level signal. This quantifies the maximum potential steepness attainable at the envelope maximum. In the present study, the measured S value for each run was determined just before the first break, in order to exclude the viscous background loss. A detailed discussion of this process is given in §4.3. To quantify the mean energy dissipation rate due to breaking, and the breaking strength coefficient b in (1.1) from this data, we used the procedure described in Appendix A.

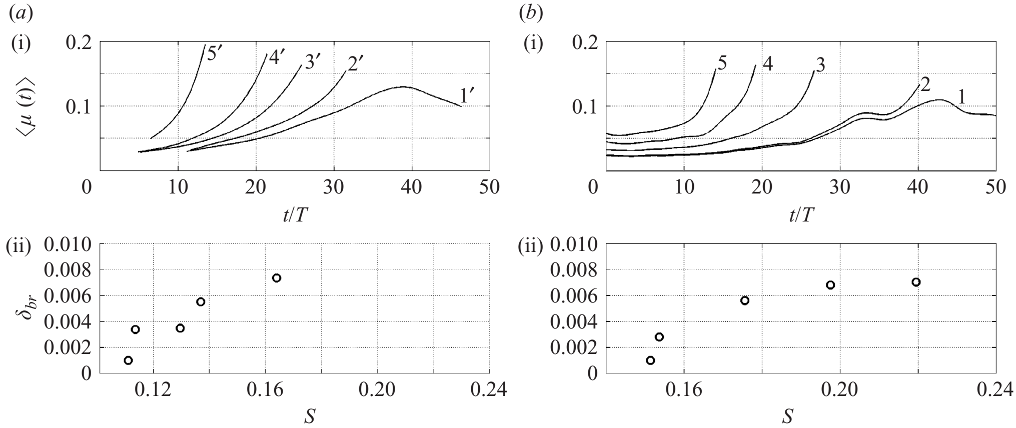

FIGURE 5. (*a*) Composite of the observed evolution curves for the mean energy $\langle\mu\rangle$ for different initial maximum steepness levels S of case II, $N = 5$ wave groups (i) and their corresponding growth rates δ_{br} just before breaking inception (ii). The identifiers 1′–5′ indicate increasing order of S (*b*) corresponding computed results as presented in figure 12 of SB, withidentifiers 1–5 indicating increasing order of S. Owing to the differential frictional attenuation between the cases, the values of S in the experiments were measured just before breaking onset. The lowest S value in (ii) corresponds to the maximum recurrence case, with its maximum growth rate.

4. Results

4.1. *Evolution properties*

Figures 3(*a*)(i) and (ii) and 4(*a*)(i) and (ii) show the measured evolution behaviour of the wave elevation and the local wavenumber at the successive group crest and trough maxima. Figure 3 shows the maximum recurrence case and figure 4 shows the marginal breaking case, obtained by increasing incrementally the initial mean carrier wave steepness until breaking initiation was evident visually. Figures 3(*a*)(iii) and 4(*a*)(iii) show the corresponding evolution of μ at these maxima and minima, and also the calculated evolution of its average value, $\langle\mu\rangle$, after smoothing out the fluctuations due to the crest and trough maxima, calculated from the average of the smoothed spline fits to the crest and trough maxima. This follows the methodology described in detail in Appendix B of SB. Figures 3(*a*)(iv) and 4(*a*)(iv) show the calculated non-dimensional growth rate δ, which reflects the mean convergence rate of energy to (or from) the group maximum.

The major points of comparison are the non-dimensional energy μ values and non-dimensional evolution times t/T (T is the mean carrier wave period), either at the recurrence maximum, or at the breaking onset time T_{br}. It can be seen that the key values of the mean growth rate δ, either at the recurrence maximum or at breaking onset, conform closely to the computed values. The recurrence cases have maximum growth rates below the SB breaking threshold of $(1.4 \pm 0.1) \times 10^{-3}$, whereas the marginal breaking cases exceed this threshold close to breaking onset.

Figure 5(*a*) summarizes the ensemble of measured $\langle\mu\rangle$ evolution curves as the initial mean carrier wave steepness is increased for the case II, $N = 5$ wave groups investigated. These are directly comparable with the upper panel in figure 12 of SB, shown in figure 5(*b*). There is close correspondence between details of the observed evolutional curves and model results. The non-dimensional time t/T to reach maximum recurrence is 42 in the model compared with 37 in the observations, with a similar number of local crest and trough maxima. This close correspondence was also found for the case II, $N = 3$ evolution results, with the non-dimensional time t/T to maximum recurrence of 24.0 in the observations compared with 23.4 in the model, again with a similar number of local crest and trough maxima.

On the other hand, the modelled and observed evolutions for the case III wave groups were significantly different, especially in terms of non-dimensional evolution time to maximum recurrence. As discussed in the last paragraph in § 2.2, we attribute this to the mismatch of initial wave-generation conditions in the model and experiment. This was confirmed some time after these experiments were concluded when the flexible paddle had been replaced by a piston paddle to carry out a shallow-water study. A quick test using the ensemble of case II, $N = 3$ wave groups showed the marginal break point shifted from 8.7 m for the flexible paddle to 14.3 m for the piston paddle. Thus, a detailed quantitative comparison of the calculated and observed evolution details with respect to t/T behaviour was not pursued for the case III groups.

4.2. *Breaking initiation threshold*

One of the major aims of this study was to investigate, for a range of wave group geometries, the behaviour of the parametric energy convergence rate δ with increasing values of the initial carrier wave steepness, commencing with the marginal recurrence evolution case. These results are shown in figures 3(*a*)(iv) and 4(*a*)(iv). These results show that the maximum value attained by $\delta(\mathrm{t})$ for recurrence remains below the common breaking threshold value $(1.4 \pm 0.1) \times 10^{-3}$ proposed by SB. Each of the subsequent runs in which the initial mean carrier wave steepness (S) was increased progressively, such as is illustrated in figure 5(*a*), experienced breaking onset once that threshold level was exceeded, with a systematic decrease in both the time that the breaking threshold was first exceeded and the breaking onset time. These generic trends are evident for each of the wave group cases II and III investigated, and mirror the behaviour of the model calculations in SB. Table 1 summarizes the salient features of each of the cases investigated in this study.

From their modelling study, SB noted that the proposed convergence-based breaking criterion allows advance notice of breaking initiation. This was confirmed in the present set of observations. For example, in the case shown in figure 4, the breaking threshold is exceeded at $t/T \sim 28$, whereas breaking initiation occurs at $t/T \sim 32$. The appropriate entries in table 1 show similar behaviour for each of the other cases observed.

We made an assessment of the likely strength of viscosity effects on breaking initiation. Following Tulin & Waseda (1999, § 3.2.3), the spatial amplitude decay rate $\mathrm{d}(\ln(a))/\mathrm{d}(kx)$ for linear waves is dominated by the sidewall interaction and is given by $\beta_D = (2\nu/\omega)/B$, where a is the wave amplitude, x is the streamwise fetch, k and ω are the wavenumber and frequency, ν is the kinematic viscosity of water and B is the tank width. For $\nu \sim 10^{-6}\,\mathrm{m^2\,s^{-1}}$ and $B = 0.6\,\mathrm{m}$, $\beta_D \sim 8 \times 10^{-4}$ and the corresponding energy decay rate is $\beta_E \sim 1.6 \times 10^{-3}$. This translates into a loss of mean wave energy of about 20 %, or a reduction of about 2 mm in the wave amplitude (from 22 mm to 20 mm) over the recurrence interval $10 < t/T < 47$ in the wave tank.

To assess its significance on the measurements of parametric growth rates δ, β_E must be transformed to have the same growth rate form as $\delta = (1/\omega_c)(\mathrm{D}\langle\mu\rangle/\mathrm{D}t)$, where $\mu = k^2 E_{loc}$ and E_{loc} is the depth-integrated potential plus kinetic energy. This transformation is straightforward and results in β_E being reduced by the factor μ/π. Even for the largest value of $\mu \sim 0.2$, the transformed β_E is 1.3×10^{-4}, which is

Case II, $N = 5$ $c_g = 0.545$	S	δ_{br} or δ_{max}	$\langle E_0 \rangle$ (m^2)	$\Delta\langle E \rangle$ (m^2)	$\langle X_T \rangle$ (m)	$\langle X_b \rangle$ (m)	b
0143(rec)	1.19×10^{-1}	0.99×10^{-3}	–	–	–	–	–
0146(mb)	1.13×10^{-1}	3.35×10^{-3}	2.15×10^{-4}	4.95×10^{-6}	4.9	3.2	8.24×10^{-5}
0155(wb)	1.26×10^{-1}	3.47×10^{-3}	2.48×10^{-4}	1.56×10^{-5}	4.9	3.56	2.60×10^{-4}
0175(ib)	1.34×10^{-1}	5.50×10^{-3}	2.95×10^{-4}	3.63×10^{-5}	5.75	4.04	6.04×10^{-4}
019(sb)	1.63×10^{-1}	7.60×10^{-3}	4.20×10^{-4}	7.35×10^{-5}	7.4	5.58	1.22×10^{-3}
Case II, $N = 3$							
$c_g = 0.563$							
0168(rec)	1.34×10^{-1}	1.10×10^{-3}	–	–	–	–	–
0169(mb)	1.33×10^{-1}	2.00×10^{-3}		-			
0174(wb)	1.56×10^{-1}	3.41×10^{-3}	3.60×10^{-4}	1.76×10^{-5}	3.20	2.24	2.53×10^{-4}
0187(ib)	1.58×10^{-1}	4.78×10^{-3}	4.00×10^{-4}	3.76×10^{-5}	3.59	2.37	6.36×10^{-4}
0195(sb)	1.66×10^{-1}	5.25×10^{-3}	4.40×10^{-4}	4.54×10^{-5}	5.2	3.12	7.35×10^{-4}
Wide basin							
rec	1.51×10^{-1}	0.40×10^{-3}	–	–	–	–	–
mb	1.52×10^{-1}	2.80×10^{-3}	3.74×10^{-4}	–			–
wb	1.54×10^{-1}	3.62×10^{-3}	3.81×10^{-4}	1.58×10^{-5}	3.8	2.85	2.63×10^{-4}
sb	1.74×10^{-1}	4.92×10^{-3}	4.17×10^{-4}	3.05×10^{-5}	4.2	2.8	5.07×10^{-4}
Case III, $N = 5$							
$c_g = 0.60$							
050(rec)	0.1198	1.14×10^{-3}	–	–	–	–	–
0508(mb)	0.1211	2.27×10^{-3}	4.68×10^{-4}	–	4.4	2.63	–
052(ib)	0.1246	2.83×10^{-3}	4.95×10^{-4}	1.19×10^{-5}	4.8	3.08	1.38×10^{-4}
053(sb)	0.1234	3.98×10^{-3}	5.25×10^{-4}	2.57×10^{-5}	4.6	3.67	2.98×10^{-4}

TABLE 1. Summary of main observational results. The column entries from left to right are as follows: wave group case type (rec, maximum recurrence; mb, wb, ib, sb are marginal, weak, intermediate and strong breaking), showing mean linear group speed c_g; maximum wave group steepness parameter S; growth rate just prior to breaking, δ_{br}, maximum growth rate during recurrence, δ_{max}; $\langle E_0 \rangle$ is the mean wave packet energy just before breaking onset; $\Delta\langle E \rangle$(m^2) is the total change in mean wave packet energy associated with breaking; $\langle X_T \rangle$ (m) is the total distance from the initiation to the cessation of breaking; $\langle X_b \rangle$ (m) is the total distance fetch along which active breaking occurs; b is the breaking strength coefficient.

an order of magnitude smaller than 1.4×10^{-3}, the breaking threshold growth rate for δ. Consequently, frictional losses were not judged to be critical for the breaking initiation phase of the investigation. This conclusion was confirmed subsequently in the auxiliary wide wave basin experiment for case II, $N = 3$ wave groups, where the results were very similar to those for the 0.6 m wide wave channel.

4.3. *Extraction of breaking losses and loss rates*

As described above, the computations in SB could not proceed past the point of breaking onset, so we were especially interested in the post-breaking measurements. It was an important goal of this study to determine the associated breaking energy losses and loss rates, and to correlate these with the proposed dynamical variable δ_{br}, as well as with more traditional measures such as the initial maximum wave steepness S used in previous wave-tank studies (e.g. Rapp & Melville 1990), but for which a field counterpart arguably does not exist. The role played by viscous losses was a significant factor in our wave-tank estimates of mean total energy losses of the group associated with the breaking process.

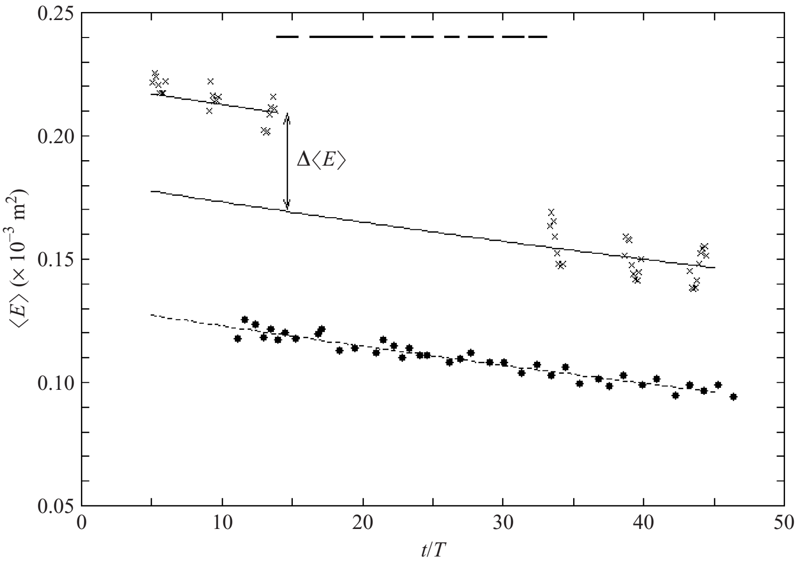

FIGURE 6. The energy loss determination procedure, shown for the strongest case II, $N = 5$ wave group evolution through breaking. The lower set of data points ($*$) shows the background frictional attenuation of the wave packet mean energy $\langle E \rangle$ for the recurrent case II, $N = 5$ wave groups. The upper set of data points ($\times$) shows, for the steepest initial case II, $N = 5$ wave groups, the initial frictional attenuation, then the packet energy loss due to a sequence of active breaking events (indicated by the dashed lines at the top of the figure, from $t/T = 14$ to 33), then the frictional attenuation of the post-breaking packet energy. The calculation details are given in the text.

The change in mean potential energy for each of the wave group cases was measured during the evolution, upstream and downstream of the sequence of multiple breaking events. The recurrence case acted as the background reference, with the energy loss attributable to viscosity alone. By making use of the ambient attenuation both upstream of the first break and also for the recurrence cases, these data allow estimates to be made of the mean total energy loss of the group owing to breaking after viscous losses have been taken into account. Here, it is noted that the observed attenuation rates for the recurrent nonlinear wave group evolution cases were comparable in magnitude with the viscous loss estimates based on linear wave theory given in § 4.2. However, it was observed that a log–linear plot of the mean energy decay with fetch was nonlinear. After some effort, it was found that optimal results were obtained using a quadratic least-squares fit in linear space for the background viscous loss over the fetch involved. This same trend was used as the baseline for the breaking cases, both upstream and downstream of the fetch containing the multiple breaking events. The ‘jump’ in mean energy level referenced to this baseline was deemed to provide a consistent estimate of the energy loss due to breaking. In this study, the measured loss in mean wave energy density ranged up to 17.1 % of the pre-breaking energy density level. Representative results are shown in figure 6, and the full set of results documenting the observed breaking properties is recorded in table 1. In addition to the absolute breaking losses, the observed breaking durations allow estimation of the wave energy dissipation rate ε associated with active breaking, as calculated according to the methodology in Appendix A.

Figures 7(a) and 7(b) show for all wave group cases investigated the breaking energy loss fraction and the breaking strength coefficient b in (1) for the breaking dissipation

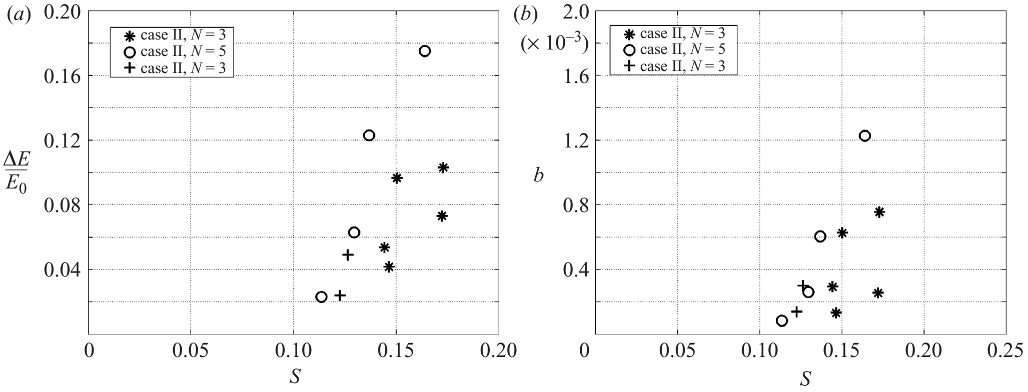

FIGURE 7. Measured dependence on the initial maximum steepness parameter S of (*a*) the relative energy loss due to breaking and (*b*) the breaking strength parameter b, defined in (A 2). Because of the differential frictional attenuation between the cases, the values of S in the experiments were measured just before breaking onset.

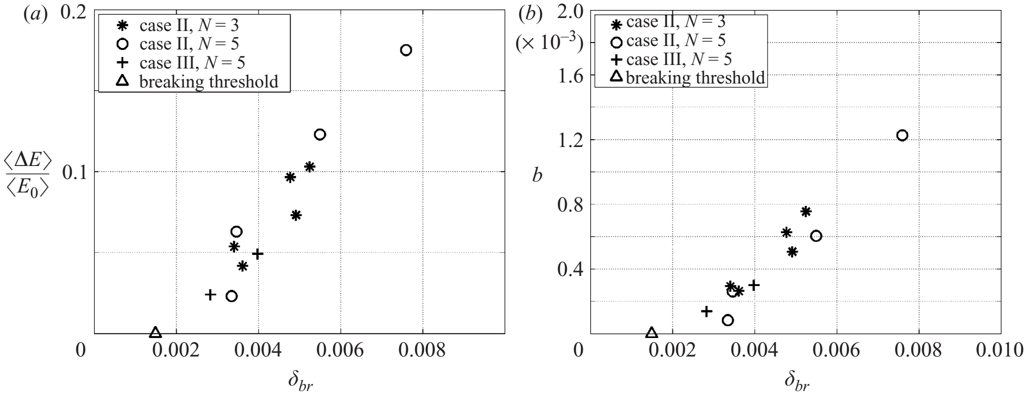

FIGURE 8. Measured dependence on the growth rate parameter δ_{br} of (*a*) the relative energy loss due to breaking and (*b*) the breaking strength parameter b, defined in (A 2).

rate ε per unit breaker width, as a function of the initial mean wave steepness S. Owing to viscous losses, S was higher at the wave paddle than in the model runs. Hence, we allowed for this by calculating S just before breaking onset, and for the fetch corresponding to the maximum recurrence for that particular case.

An alternative, and arguably more fundamental, presentation of this data is to compare the observed fractional loss $\Delta E/E_0$ and the breaking strength parameter rate coefficient b_{br} with the observed growth rate δ_{br} just before breaking onset. SB anticipated that this would provide a more intrinsic measure of strength of breaking. The results for these correlations are shown for the cases investigated in figure 8. It is clear that the behaviour for case II and III wave groups is very similar and the data points for each of the cases fall, within experimental scatter, along a common curve. Moreover, this curve is closely aligned with the breaking threshold growth rate δ_{th}.

5. Discussion

Based on the detailed comparison of evolutional properties of the case II wave groups with the model predictions of SB, we observed for both the computed and observed evolutions that approximately the same number of the distinctive local maxima (both crest and trough) occur in the evolution to the recurrence maximum. The same behaviour occurred for the evolution to marginal breaking. For increasing initial group steepness S, the observed evolution continued to mirror the key features of the computations: decreasing t/T to reach the breaking threshold growth rate transition, and steadily increasing $\delta(t)$ thereafter, until breaking onset.

Also, the dynamic range of $\langle\mu\rangle$ during the evolution to the recurrence maximum was from 0.025 to 0.11 in the model and from 0.025 to 0.14 in the observations. The corresponding evolution time to the recurrence maximum was approximately $42T$ for the model compared with $37T$ in the observations. This is consistent with the slightly higher observed growth rates $\delta(t)$ compared with the corresponding inviscid model results.

In summary, the observed evolution of case II wave groups closely parallels the model results, with the observational evolution occurring slightly faster in terms of t/T. In this regard, we note that the values for the initial wave group steepness S for model and observations were, respectively, 0.015 and 0.0185. We attribute the steeper initial wave group required in the wave tank to compensate for the viscous losses in the wave tank. With the steeper initial wave group required to offset the frictional effects, it is envisaged that the nonlinear evolution proceeds proportionally faster, which is consistent with the observed differences.

5.1. *Predicting breaking onset*

Validating breaking onset in terms of a threshold of $\delta(t)$ in the range $(1.4 \pm 0.1) \times 10^{-3}$ was one of the primary goals of this study. This was observed in each of the cases of wave groups investigated in this study. This result provides, for the first time as far as we are aware, a non-local predictor for breaking onset that is based on wave energetics and can anticipate breaking onset in advance of its actual onset. Typically, there are up to several periods between $\delta(t)$ exceeding the breaking threshold and the onset of active breaking.

5.2. *Strength of breaking*

SB proposed that the breaking strength might be strongly correlated with $\delta(t)$ just prior to breaking, denoted by δ_{br}. This key proposal from the SB model results was validated convincingly in our observations (figure 8).

We found that the downstream mean energy density after breaking had ceased, was considerably higher than the mean energy density for the respective maximum recurrent cases. This indicates that the maximum recurrence energy density is not the primary determinant for the post-breaking energy density.

Finally, it should be noted that in this study, the breaking onset in each case resulted in multiple (successive) breaks. The maximum observed relative breaking energy loss ratios $\Delta E/E_0$ were somewhat lower than in Melville (1994), because of the different initial wave group configurations investigated. Melville (1994, p. 2047) associates multiple breaking with higher values of S. We envisage that the occurrence of a single strong break as opposed to multiple weak breaks is also related to the level attained by δ_{br}. However, we are unable to confirm this from our present observations in which no single break cases occurred. It should also be noted that when three-dimensional effects are included in the wave field, directional wave crest convergence (divergence) enhances (reduces) breaking energy losses and strength (e.g. Nepf, Wu & Chan 1998). Hence, the present two-dimensional wave breaking results should be extended in a future study to embrace the effects of wave breaking directionality.

5.3. *Comparison with available field observations*

In this study, the breaking strength coefficient has been defined in relation to the linear wave speed c, as in (A 2), rather than the actual breaker crest speeds c_{br} that have been used to date. This breaker strength coefficient is designated b, in contrast to b_{br} defined in (2). The underlying motivation is related to self-consistent transformation, as discussed in detail in Appendix A § A 2. For the breaking waves in this laboratory study, we found values of b ranging between 8×10^{-5} and 1.2×10^{-3}, with a near-linear dependence on the convergence rate parameter δ_{br}. Since $c_{br} \sim (0.8\text{–}0.9)c$, it is easily seen that $b \sim \mathrm{O}[(0.85)^5]\ b_{br} \sim 0.5 b_{br}$.

From their analysis of radar field data, Phillips *et al.* (2001) reported $b_{br} \sim (0.7\text{–}1.3) \times 10^{-3}$. Allowing for the $O(0.5)$ factor quoted in the previous paragraph, these levels are comparable with those found in our laboratory study. On the other hand, Melville & Matusov (2002) quote a representative value of $b_{br} \sim 8 \times 10^{-3}$ which appears to have been inferred from laboratory data estimates of b_{br} in the range $(3\text{–}16) \times 10^{-3}$ (Melville 1994). After rescaling by 0.5 (see discussion at the end of previous paragraph), these values are about an order of magnitude higher than were found for the spilling breakers in the present study.

In any event, for two-dimensional wave groups, we have observed a strong dependence of b on the rate of energy convergence and geometrical steepening just prior to breaking. In the field, breaking occurs in more complex wave group systems, and over a wide range of wave scales (e.g. as measured by their speed c), with potentially different convergence rates. Determining whether other parameters should be included to more accurately characterize b remains to be explored in future studies.

5.4. *Comparison of the present modulational growth rates and dissipation rates with other air–sea interaction growth rates*

It is of interest to compare the characteristic mean growth rates and breaking loss rates observed in this study with characteristic growth rates in the closely related problem of wind–wave generation. Banner & Song (2002) found that the impact of wind forcing was secondary compared to hydrodynamic wave group evolution effects, even for relatively strongly forced cases. Hence, the unforced results are assumed to be representative of the wind-driven case, and will be used in the following comparison.

From the discussion in § 1.1, we recall that the definition of $\delta = (1/\omega_c)(\mathrm{D}\langle\mu\rangle/\mathrm{D}t)$, where $\mu = Ek^2$, differs from the usual non-dimensional relative growth rate $(1/\omega_c E)(\mathrm{D}E/\mathrm{D}t)$. From our measurements, the latter is found to be $O(0.05\text{–}0.10)$. This was inferred using a similar procedure to that described in § 4.2, using typical values of the variables shown in the figures. Also, the observed dissipation rate associated with the active periods of the multiple weak spilling breaking events in our experiments was found to be $O(0.005)$. In comparison, for the wind-driven problem, Donelan (1999) reported relative growth rates due to wind input ranging up to $O(0.01)$ for very strong generating conditions (typically the wind speed was seven times larger than the wave speed), with a dissipation rate due to breaking of the same order of magnitude. Hence, it is seen that if the mean wave steepness is $O(0.1)$, the group-mediated hydrodynamic energy fluxes can make a relatively strong contribution on the short time scale. However, while local wave group modulation is believed to be operative generally, it is tacitly assumed in spectral wind wave evolution models that its net influence averages to zero over longer times. On the other hand, wave breaking, including the group-mediated contribution, is thought to be the major contributor to the dissipation rate source term that describes the spectral mean loss rate of wave energy. This term should also include a background wave energy loss rate associated with turbulence in the wave boundary-layer region. However, at present there is a lack of consensus on the form of this term.

Given that spectral wave models do not resolve wave groups explicitly, the task of including the above contributions is a significant challenge. Alves & Banner (2003) attempted to encapsulate the breaking contribution parametrically in a spectral dissipation source term premised on a breaking threshold that uses the spectral saturation as a surrogate for δ. This choice was motivated by the relationship between the spectral saturation, integrated over a logarithmic wavenumber bandwidth, and the corresponding mean wave steepness, a classical measure of wave nonlinearity. Notwithstanding certain conceptual issues, the use of the spectral saturation as a viable breaking threshold parameter was investigated in detail in ocean storm wave measurements by Banner, Gemmrich & Farmer (2002). Others such as Badulin *et al.* (2005), have proposed substantially different perspectives on the nature and spectral representation of wave dissipation. However, resolving this issue is well beyond the scope of the present contribution.

6. Conclusions

The major conclusions of this investigation for wave breaking onset are as follows.

(i) For both breaking and recurrence, the depth-integrated local energy density following the maximum of the wave group was observed to evolve in a complex fashion, with a 'fast' oscillation superimposed on a longer-term mean trend. This behaviour closely parallels the computational results reported in SB. In relation to breaking onset, the 'fast' oscillation, due to the strong crest/trough asymmetry of the carrier waves, is believed to be primarily a kinematic effect. A non-dimensional parametric growth rate $\delta(t)$ was derived from the mean trend of the diagnostic parameter $\mu(t)$, which reflects the systematic mean wave energy convergence and carrier wave steepening towards the maximum energy region within the wave group. This growth rate appears to determine the ultimate breaking or recurrence behaviour.

(ii) Our measurements support the findings of the SB calculations that breaking or recurrence for two-dimensional chirped or unstable sideband deep water wave groups are determined by a common growth rate threshold δ_{th} that is independent of the initial wave group structure. The numerical study of SB found that δ_{th} lay in the range $(1.4 \pm 0.1) \times 10^{-3}$. For the cases investigated in this study, recurrence behaviour occurred for a maximum value of $\delta(t)$ that lies below this threshold, and decreased thereafter. This is in contrast with the breaking cases investigated, where $\delta(t)$ continued to increase after it reached this threshold level, after which breaking occurred within a time interval ranging up to several carrier wave periods. Thus, using the growth rate δ provides an advance warning time of imminent breaking of up to several carrier wave periods prior to breaking onset. To our knowledge, this is unmatched by any previously proposed breaking onset predictor.

The major conclusions of this investigation for wave breaking strength are as follows.

(iii) The strength of breaking events is strongly correlated with the mean rate of convergence of energy and carrier wave steepening at the group maximum immediately preceding breaking onset, as reflected by δ_{br}, the corresponding value of $\delta(t)$ just preceding breaking onset. For the two classes of wave groups investigated, an excellent collapse of the data was found between δ_{br} and the breaking-induced fractional energy loss, with significantly less scatter than for correlations based on initial wave packet steepness.

(iv) The post-breaking mean energy density was found to remain significantly above the maximum energy density for maximal recurrent wave groups, which have comparable local geometric and energetic waveforms. This further reinforces the hypothesis that breaking is more closely linked to wave energy convergence rates rather than absolute local wave energy levels.

(v) The breaking strength parameter b in equation (A 2) for the dissipation rate per unit breaker crest length was deduced from measurements of the post-breaking energy loss process. The results from the different cases collapsed on a common trend. The breaking strength parameter b ranged from 8×10^{-5} to 1.2×10^{-3} and was found to have a strong near-linear dependence on the growth rate parameter δ_{br}.

(vi) This study provides encouraging initial observational support for the nonlinear wave-group mediated onset of breaking within two-dimensional nonlinear wave groups. The relevance of this approach to breaking onset and strength for field wave groups, which includes three-dimensional effects that are known to occur in the open ocean, remains to be investigated. Other related fundamental issues work to be resolved in future include understanding what determines the frequently observed occurrence of multiple successive breaking events in a wave group.

This study has significant implications for future wave observational research. The present generation of spectral wind wave models does not explicitly incorporate wave group effects. Energy convergence rates within wave groups may be several times stronger than the wind input. This was seen in the numerical study of Banner & Song (2002), but is also evident in recent field observations of maturing wind seas. These have relatively weak wind forcing at the spectral peak, yet are sufficiently steep for nonlinear effects to produce breaking of the dominant waves (e.g. see the top left-hand panel in figure 3 in Gemmrich 2005). This study highlights the need to gather space–time information that embraces evolving wave groups in order to improve our present knowledge of wave breaking. Such instrumentation capabilities are becoming available and should be able to provide new insight into these key processes.

The financial support of the Australian Research Council and a University of New South Wales Gold Star award for this project is gratefully acknowledged, together with the expert assistance of the workshop staff at the UNSW Water Research Laboratory. During the course of the project the technical assistance of Chris Adamantidis, Ainslie Fraser, Rowan Hudson, David Dack, Evan Watterson and Ian Coghlan with the measurements, and of Dr. Jinbao Song and Russel Morison with the data analysis, was instrumental in the execution and success of this study. MLB also acknowledges the ongoing support from the US Office of Naval Research during this investigation.

Appendix A. Estimating the breaking strength parameter *b*

A.1. *Background*

Originally developed for quasi-steady breaking, Duncan (1981, 1983) introduced the mean energy density dissipation rate per unit length of breaking crest ε_L:

$$\varepsilon_L = b_{br}\rho_w c_{br}^5/g. \tag{A 1}$$

The unknown coefficient b_{br} quantifies the breaking strength, c_{br} characterizes the speed of the breaking wave and ρ_w is the water density. Phillips (1985) applied this form subsequently for transient breaking in a spectral context. There is a complementary form for the momentum flux transferred by the breaker to the subsurface flow that involves the fourth power of c_{br}.

Equation (A 1) is based on the mean rate of working of a breaker of cross-sectional area A_b and propagation speed c_{br} against the orbital motion of the underlying wave. In unsteady breaking, c_{br} and A_b are time-dependent, and further assumptions are invoked. A_b is assumed to maintain a constant aspect ratio, i.e. proportionality to λ^2, the square of the wavelength of the breaking wave; a dispersion relation is assumed between λ and c_{br} which allows A_b to be expressed in terms of c_{br}. The coefficient b_{br} in (A 1) incorporates these unsteady aspects.

Several authors have provided estimates for c_{br} in relation to the corresponding linear wave speed c of the other less steep waves in the group. For their ocean whitecap measurement analysis, Melville & Matusov (2002) adopted $c_{br} = 0.80c$, while for microscale breakers, Jessup & Phadnis (2005) reported $c_{br} = \gamma c$, where γ varied over the range $0.22 < \gamma < 0.85$, according to the analysis methodology and cases investigated. In the present study, measured values of $c_{br} = (0.9 \pm 0.05)c$ were found (see Appendix B below). In this context, note that for wave packets about to break, the departure from the linear wave speed c can be associated with the unsteady nonlinear distortion of the maximal wave in the packet. The local wavelength and wave period of the breaking wave contract owing to the nonlinearity. The effect is seen in figure A 2(*a*) of SB.

A.2. *Transformation properties*

Note that the choice of c_{br} in (A 1) has certain associated implications that have not been considered previously. These arise in relation to using this parameterization of the impact on breaking-induced dissipation rates and momentum fluxes in spectral wave model applications.

The issue of the most appropriate form for (A 1) arises in the context of estimating spectral energy dissipation rates and momentum impulse contributions from breaking waves in the field (e.g. Melville & Matusov 2002; Gemmrich 2005). Typically, video imagery of the sea surface allows extraction of the spectral density of mean breaking crest length Λ as a function of the observed breaker speed c_{br}. However, the usual spectral wave description is expressed in terms of linear Fourier mode speed c (or the equivalent frequency or wavenumber given by the linear wave dispersion relation), and a difficulty arises with the transformation if (A 1) is based on a c_{br} dependence.

In essence, the total energy dissipation rate ε and momentum impulse I contributions from breaking waves involve fifth and fourth moments, respectively, of the Λ distribution, i.e.

$$\varepsilon = \int b g^{-1} c^5 \Lambda(c)\, \mathrm{d}c, \qquad I = \int b g^{-1} c^4 \Lambda(c)\, \mathrm{d}c.$$

The breaker image sequence measurements deliver estimates of $\Lambda(c_{br})$, whereas the models use $\Lambda(c)$. These two forms are readily transformed by requiring the total integrated crest length to be conserved, hence $\Lambda(c) = \Lambda(c_{br})\mathrm{d}c_{br}/\mathrm{d}c$. Assuming that $c_{br} \sim \gamma c$ (see Appendix B), this transformation is straightforward. Further, it can be seen that the energy and momentum fluxes transform consistently if they are based on c, but this no longer holds if they are based on c_{br}. On this basis, we recommend adopting the form

$$\varepsilon_L = b \rho_w c^5 / g, \tag{A 2}$$

and the following data analysis for quantifying b from the wave tank data in this study is based on this equation.

A.3. *Determination of b from the data*

The water density ρ_w is suppressed in the analysis that follows, which describes how b was determined from the energy loss measurements in this study. The measured mean energy density loss between the initiation and final cessation of breaking is $\Delta\langle E\rangle$, where $E = g\eta^2$ is the wave energy density, and $\langle..\rangle$ denotes the average over the wave group. This energy density loss associated with a given (multiple) breaking event was deemed to occur over a set of active breaking sub-fetches of total length X_{AB}. The active breaking width was observed to extend approximately uniformly across the tank width W.

For the quasi-steady conditions in the tank for the mean properties of the wave groups, the wave energy propagation equation for $\langle E\rangle$ reduces to

$$D\langle E\rangle Dt = c_g \mathrm{d}\langle E\rangle \mathrm{d}x = S_{ds}, \tag{A 3}$$

where S_{ds} is the mean rate of loss of the energy density of the wave group through breaking.

For S_{ds}, we take (A 2), and apply it to the actively breaking front that extends across the tank width W. In order to express this per unit area, we divide by the swept breaking area $X_{AB}W$. Thus, the mean rate of energy loss over the fetch X_{AB} is given by

$$bc^5/g \times W/(X_{AB}W). \tag{A 4}$$

Next, expressing (A 3) as a finite-difference gradient across the active breaking extent X_{AB} over which fetch the mean energy breaking loss is $\Delta\langle E\rangle$ gives the mean energy loss rate per unit area

$$c_g\Delta\langle E\rangle/X_{AB}, \tag{A 5}$$

Equating (A 4) and (A 5) and solving for b gives

$$b = gc_g\Delta\langle E\rangle/c^5 \tag{A 6}$$

Equation (A 6) was used to determine b for each of the cases measured in this study. It is noteworthy that this result is independent of whether the breaking occurs as a single break or a multiple succession of breaks. It is also independent of the actual breaker speed relative to the linear phase speed.

Table 1 shows that the mean breaking strength coefficient b spans the range from 8×10^{-5} to 1.2×10^{-3}. The dependence of b on wave properties is taken up in §5.2 and §5.3 of the text.

Appendix B. Indicative measured values of breaker speed c_{br}

For interest, a small subset of wave height probe array data sets were collected downstream of the breaking initiation point from the wave probe array measurements made in this study. The sequence of time series at the two sets of three closely spaced fixed wave wire probes allowed estimation of the speed of breaking crests relative to the corresponding linear phase speed, c_{br}/c.

The following data were crest maxima with active breaking crests for the steepest (019) case II, $N = 5$ packets (see table 1). Time series of the wave heights were analysed of the upstream and downstream probes, separated by 0.1575 m (approximately 20 % of the carrier wave length). Based on a sample size of 30 waves, crest passage transit times were measured at $(20 \pm 0.7)/125$ s for the steep breaking wave at the centre of the group, and $(19 \pm 1)/125$ s for the lower steepness waves towards the end of the wave group. Hence, the respective phase speeds were $0.98 \pm 0.04\,\mathrm{m\,s^{-1}}$ and

$1.04 \pm 0.55\,\mathrm{m\,s^{-1}}$. The latter is within the experimental scatter of the linear phase speed of $1.092\,\mathrm{m\,s^{-1}}$ whereas the former gives the estimate $\gamma = c_{br}/c = 0.9 \pm 0.04$ based on the paddle frequency, and within the noise of the observed wave speed. The observed reduction in breaker speed is appreciably less than that reported by Melville & Matusov (2002) and Jessup & Phadnis (2005).

REFERENCES

Alves, J. H. & Banner, M. L. 2003 Performance of a saturation-based dissipation source term for wind wave spectral modelling. *J. Phys. Oceanogr.* **33**, 1274–1298.

Badulin, S. I., Pushkarev, A. N., Resio, D. & Zakharov, V. E. 2005 Self-similarity of wind driven seas. *Nonlinear Proc. Geophys.* **12**, 891–945.

Banner, M. L. & Peregrine, D. H. 1993 Wave breaking in deep water. *Annu. Rev. Fluid Mech.* **25**, 373–397.

Banner, M. L. & Song, J. 2002 On determining the onset and strength of breaking for deep water waves. Part 2: Influence of wind forcing and surface shear. *J. Phys. Oceanogr.* **32**, 2559–2570.

Banner, M. L. & Tian, X. 1998 On the determination of the onset of breaking for modulating surface gravity water waves. *J. Fluid Mech.* **367**, 107–137.

Banner, M. L., Gemmrich, J. R. & Farmer, D. M. 2002 Multiscale measurements of ocean wave breaking probability. *J. Phys. Oceanogr.* **32**, 3364–3375.

Dias, F. & Kharif, C. 1999 Nonlinear gravity and capillary-gravity waves. *Annu. Rev. Fluid Mech.* **31**, 301–346.

Dold, J. W. & Peregrine, D. H. 1986 Water–wave modulation. *Proc. 20th Intl Conf. Coastal Engng Taipei, ASCE* vol. 1, pp. 163–175.

Donelan, M. A. 1999 Wind-induced growth and attenuation of laboratory waves. In *Wind over Wave Couplings* (ed. S. G. Sajjadi, N. H. Thomas & J. C. R. Hunt, Clarendon), pp. 183–194.

Donelan, M. A., Longuet-Higgins, M. S. & Turner, J. S. 1972 Whitecaps. *Nature* **239**, 449–451.

Duncan, J. H. 1981 An experimental investigation of breaking waves produced by towed hydrofoil. *Proc. R. Soc. Lond.* A **377**, 331–348.

Duncan, J. H. 1983 The breaking and non-breaking resistance of a two-dimensional hydrofoil. *J. Fluid Mech.* **126**, 507–520.

Dysthe, K. B. 1979 Note on a modification to the nonlinear Schrödinger equation for application to deep water waves. *Proc. R. Soc. Lond.* A **369**, 105–114.

Gemmrich, J. 2005 On the occurrence of wave breaking. *Proc. Hawaiian Winter Workshop on Rogue Waves* (ed. P. Muller & D. Henderson), pp. 123–130. University of Hawaii SOEST.

Gemmrich, J. R. & Farmer, D. M. 2004 Observations of the scale and occurrence of breaking surface waves. *J. Phys. Oceanogr.* **34**, 1067–1086.

Holthuijsen, L. H. & Herbers, T. H. C. 1986 Statistics of breaking waves observed as whitecaps in the open sea. *J. Phys. Oceanogr* **16**, 290–297.

Jessup, A. T. & Phadnis, K. R. 2005 Measurement of the geometric and kinematic properties of microsacle breaking waves from infrared imagery using a PIV algorithm. *Meas. Sci. Technol.* **16**, 1961–1969.

Kway, J. H. L., Loh, Y.-S. & Chan, E.-S. 1998 Laboratory study of deep-water breaking waves. *Ocean Engng* **25**, 657–676.

Loewen, M. R. & Melville, W. K. 1991 Microwave backscatter and acoustic radiation from breaking waves. *J. Fluid Mech.* **224**, 601–623.

Longuet-Higgins, M. S. 1984 Statistical properties of wave groups in a random sea state. *Phil. Trans. R. Soc. Lond.* A **312**, 219–250.

Melville, W. K. 1982 The instability and breaking of deep-water waves. *J. Fluid Mech.* **115**, 165–185.

Melville, W. K. 1983 Wave modulation and breakdown. *J. Fluid Mech.* **128**, 489–506.

Melville, W. K. 1994 Energy dissipation by breaking waves. *J. Phys. Oceanogr.* **24**, 2041–2049.

Melville, W. K. 1996 The role of surface-wave breaking in air-sea interaction. *Annu. Rev. Fluid Mech.* **26**, 279–321.

Melville, W. K. & Matusov, P. 2002 Distribution of breaking waves at the ocean surface. *Nature* **417**, 58–63.

Nepf, H. M., Wu, C. H. & Chan, E. S. 1998 A comparison of two- and three-dimensional wave breaking. *J. Phys Oceanogr.* **28**, 1496–1510.

Osborne, A. R., Onorato, M. & Serio, M. 2000 The nonlinear dynamics of rogue waves and holes in deep water gravity wave trains. *Phys. Lett.* A **275**, 386–393.

Papadimitrakis, Y. A., Huang, N. E., Bliven, L. F. & Long, S. R. 1988 An estimate of wave breaking probability for deep water waves. In *Sea Surface Sound – Natural Mechanisms of Surface-Generated Noise in the Ocean* (ed. B. R. Kerman), pp. 71–83. Kluwer.

Peirson, W. L. & Banner, M. L. 2000 On the strength of breaking of deep water waves. In *Coastal Engineering 2000, ASCE, Sydney* (ed. R. Cox), pp. 369–381.

Phillips, O. M. 1985 Spectral and statistical properties of the equilibrium range in wind-generated gravity waves. *J. Fluid Mech.* **156**, 505–531.

Phillips, O. M., Gu, D. & Donelan, M. A. 1993 Expected structure of extreme waves in a Gaussian Sea, Part 1. Theory and SWADE buoy measurements. *J. Phys. Oceanogr.* **23**, 992–1000.

Phillips, O. M., Posner, F. L. & Hansen, J. P. 2001 High range resolution radar measurements of the speed distribution of breaking events in wind-generated ocean waves: surface impulse and wave energy dissipation rates. *J. Phys. Oceanogr.* **31**, 450–460.

Rapp, R. J. & Melville, W. K. 1990 Laboratory measurements of deep water breaking waves. *Phil. Trans. Roy. Soc. Lond.* A **331**, 735–800.

Skyner, D. 1996 A comparison of numerical predictions and experimental measurements of the internal kinematics in a deep-water plunging wave. *J. Fluid Mech.* **315**, 51–64.

Song, J. & Banner, M. L. 2002 On determining the onset and strength of breaking for deep water waves. Part 1: Unforced irrotational wave groups. *J. Phys. Oceanogr.* **32**, 2541–2558.

Stansell, P. A. & MacFarlane, C. 2002 Experimental investigation of wave breaking criteria based on wave phase speeds. *J. Phys. Oceanogr.* **32**, 1269–1283.

Terray, E. A., Donelan, M. A., Agrawal, Y. C., Drennan, W. M., Kahma, K. K., Williams, III, A. J., Hwang, P. A. & Kitaigorodskii, S. A. 1996 Estimates of kinetic energy dissipation under breaking waves. *J. Phys. Oceanogr.* **26**, 792–807.

Thorpe, S. A. 1993 Energy loss by breaking waves. *J. Phys. Oceanogr.* **23**, 2498–2502.

Tulin, M. P. & Li, J. J. 1992 On the breaking of energetic waves. *Intl J. Offshore Polar Engng* **2**, 46–53.

Tulin, M. P. & Waseda, T. 1999 Laboratory observations of wave group evolution, including breaking effects. *J. Fluid Mech.* **378**, 197–232.